

$E_u(^3E_u) \leftarrow ^1A_{1g}(3b_{1g} \leftarrow 2e_u p\sigma)$. This band should occur around $3.85 \mu\text{m}^{-1}$ in CH_3OH (Figure 3a) and be connected with the strong band at lower energy in $\text{Pt}_2\text{I}_6^{2-}(\text{CH}_3\text{OH})$, viz. $3.59 \mu\text{m}^{-1}$ (Figure 4), because both the change in transition energy and the intensity ratio between these bands are very similar to those of $\text{PdI}_4^{2-}/\text{Pd}_2\text{I}_6^{2-}$ ($3.17/3.01 \mu\text{m}^{-1}$). Hypothetically, the bands at 3.76 and $3.63 \mu\text{m}^{-1}$ (PtI_4^{2-} , 5 M $\text{H}_2\text{SO}_4(\text{aq})$) can then be assigned 1E_u , $^1A_{2u} \leftarrow ^1A_{1g}(3b_{1g} \leftarrow 3e, b_{2u})$ and its corresponding singlet-triplet (compare 2.45 and $2.07/1.84 \mu\text{m}^{-1}$ for PdI_4^{2-} in Table II and Figure 2). It is obvious that arguments against these assignments can be inferred both from the smaller band spacing (about $0.3 \mu\text{m}^{-1}$) in PtI_4^{2-} but more than twice that in PdI_4^{2-} ($3.17 \mu\text{m}^{-1} - 2.45 \mu\text{m}^{-1} = 0.72 \mu\text{m}^{-1}$) and also from the different MCD (B -term) features; cf. Figure 2 ($1/\lambda < 2.7 \mu\text{m}^{-1}$) and Figure 3. (That there should be some difference in the B terms connected with LMCT transitions in PtI_4^{2-} as compared to those for PdI_4^{2-} is expected. One of the important factors is the proximity of states of correct symmetry,²² and the energy differences between states derived from metal d - p configurations and those derived from ligand p -metal $d(3b_{1g})$ configurations are considerably smaller in PtI_4^{2-} than in PdI_4^{2-} .)

The assignment alternative (ii) has been included in Table III. Because it is uncertain and other probable alternatives exist, the

individual bands have not been assigned.

Conclusions

The spectra and spectral assignments presented in this and other studies show that the internal metal d - p assignment is well established for the PtX_4^{2-} spectra ($X = \text{Cl}, \text{Br}, \text{I}$). The presence of LMCT transitions suggested⁷ to occur besides the d - p transitions seems also justified. Obviously, a number of details are still obscure. It would be highly desirable to get spectral information from single-crystal polarization measurements and to penetrate the UV spectral region for PdI_4^{2-} and $\text{Pd}_2\text{I}_6^{2-}$ both by absorption and MCD measurements.

Acknowledgment. I am very grateful to Dr. L. I. Elding for positive criticism of this work and to B. Jönsson and E. Bredendfeldt for experimental assistance. My thanks are also due to J. Glans for the MCD measurements and to Dr. I. Nilsson for help with the calculations. Financial support from the Swedish Natural Science Research Council (NFR) is acknowledged. I am much indebted to the reviewers for their critical reading and suggestions, which have greatly improved the paper.

Registry No. PdI_4^{2-} , 16182-47-1; PtI_4^{2-} , 14349-66-7; $\text{Pt}_2\text{I}_6^{2-}$, 45632-38-0.

Contribution from the Fachbereich Chemie und Sonderforschungsbereich 127 "Kristallstruktur und chemische Bindung" der Philipps-Universität, D-3550 Marburg 1, West Germany

Anisotropic Exchange Interactions in the Copper(II) and Vanadium(IV) Dimers $[(L')\text{Cu}(\mu\text{-OH})_2\text{Cu}(L')](\text{ClO}_4)_2$ and $[(L)\text{VO}(\mu\text{-OH})_2\text{VO}(L)]\text{Br}_2$ with 1,4,7-Triazacyclononane (L) and Its N,N',N'' -Trimethyl Derivative (L'): A Single-Crystal EPR Study

A. Ozarowski[†] and D. Reinen*

Received October 25, 1985

The zero-field-splitting tensors for the spin-triplet states of Cu(II) and V(IV) dimers in the compounds $[(L')\text{Cu}(\mu\text{-OH})_2\text{Cu}(L')](\text{ClO}_4)_2$ (Ia) and $[(L)\text{VO}(\mu\text{-OH})_2\text{VO}(L)]\text{Br}_2$ (II) have been deduced from the results of EPR single-crystal and powder experiments. Parameters for Ia: $|D| = 0.9250 \text{ cm}^{-1}$, $|E| = 0.0514 \text{ cm}^{-1}$; $g_z^c \approx 2.25$, $g_y^c \approx g_x^c \approx 2.06$. Parameters for II: $|D| = 0.0037 \text{ cm}^{-1}$, $|E| = 0.0472 \text{ cm}^{-1}$; $g_z^c = 1.946$, $g_y^c = 1.975$, $g_x^c = 1.988$; $A_z^c = 76 \times 10^{-4} \text{ cm}^{-1}$, $A_y^c = 32 \times 10^{-4} \text{ cm}^{-1}$, $A_x^c = 23 \times 10^{-4} \text{ cm}^{-1}$. The derived anisotropic exchange contributions to D and E allowed estimation of the exchange integrals $J_{x^2-y^2,xy}$, which are of similar magnitude for Ia ($\approx -510 \text{ cm}^{-1}$) and II ($\approx -410 \text{ cm}^{-1}$), as expected. In contrast, published values for the exchange integrals, which were calculated from magnetic susceptibility data, are very different, namely $J_{x^2-y^2,x^2-y^2} \approx 90 \text{ cm}^{-1}$ for Ia and $J_{xy,xy} \approx 354 \text{ cm}^{-1}$ for II. The latter implies a direct $d_{xy}^1-d_{xy}^1$ interaction, while the former describes a $d_{x^2-y^2}^1-d_{x^2-y^2}^1$ superexchange interaction via the bridging oxygen atoms. Results for the green isomer Ib of the blue dimer Ia, which has a $S = 1$ ground state as opposed to the case for Ia and II, are also given.

Introduction

The nature of the exchange interactions in binuclear hydroxo-bridged transition-metal complexes has been the subject of many papers published in the last 30 years. Correlations between the structure of the dimers and the energy and type of the isotropic exchange coupling were experimentally established¹ and explained by suitable theoretical models.²⁻⁵ The anisotropic exchange effects, which contribute to the zero-field splitting of dimeric compounds, have been studied intensively only in the last few years.⁵⁻⁸ Though mainly copper complexes have been studied, a paper dealing with a hydroxo-bridged chromium dimer recently appeared.⁹ We will present below the results of a spectroscopic study of binuclear bis(μ -hydroxo)-bridged complexes, which were prepared and characterized by Wieghardt and co-workers.^{10,11} The copper(II) dimer $[(L')\text{Cu}(\text{OH})_2\text{Cu}(L')]_2(\text{ClO}_4)_2$ with the tridentate ligand N,N',N'' -trimethyl-1,4,7-triazacyclononane (L') exists in two isomeric forms.¹⁰ While the blue isomer (Ia) is

structurally well-characterized with a symmetrical bis(μ -hydroxo) bridge (Figure 1, Table I), the green isomer (Ib) seems to exhibit disorder within the unsymmetrical bridge, with possibly an oxo and H_2O ligand. The Cu^{2+} ions are five-coordinated, and the geometry corresponds to a strongly elongated square pyramid. This structural feature is in accord with predictions by a vibronic

- (1) Hodgson, D. J. *Prog. Inorg. Chem.* **1975**, *19*, 173.
- (2) Hay, P. J.; Thibault, J. C.; Hoffmann, R. J. *J. Am. Chem. Soc.* **1975**, *97*, 4884.
- (3) Kahn, O.; Briat, B. *J. Chem. Soc., Faraday Trans. 2* **1976**, *72*, 268, 1441.
- (4) Bencini, A.; Gatteschi, D. *Inorg. Chim. Acta* **1978**, *31*, 11.
- (5) Bencini, A.; Gatteschi, D. *Magnetostructural Correlations in Exchange Coupled Systems*; Gatteschi, D., Kahn, O., Willett, R. D., Eds.; D. Reidel: Dordrecht, The Netherlands, 1985; p 241. Kahn, O. *Ibid.*, p 47.
- (6) Banci, L.; Bencini, A.; Gatteschi, D.; Zanchini, C. *J. Magn. Reson.* **1982**, *48*, 9.
- (7) Banci, L.; Bencini, A.; Gatteschi, D. *J. Am. Chem. Soc.* **1983**, *105*, 761.
- (8) Bencini, A.; Gatteschi, D.; Zanchini, C. *Inorg. Chem.* **1985**, *24*, 700.
- (9) Kremer, S. *Inorg. Chem.* **1985**, *24*, 887.
- (10) Chaudhuri, P.; Ventur, D.; Wieghardt, K.; Peters, E. M.; Peters, K.; Simon, A., to be submitted for publication.
- (11) Wieghardt, K.; Bossek, U.; Volckmar, K.; Swiridoff, W.; Weiss, J. *Inorg. Chem.* **1984**, *23*, 1387.

[†] On leave from the Institute of Chemistry, Wrocław University, Wrocław, Poland.

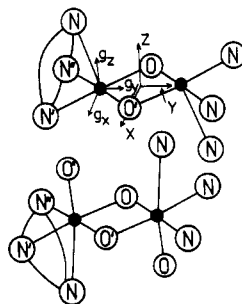


Figure 1. Schematic geometry of the dimeric entities in the compounds $[(L')Cu(OH)_2Cu(L')](ClO_4)_2$ (Ia) (above) and $[(L)VO(OH)_2VO(L)]Br_2$ (II) (below). The main axes Z and Y of the D tensor were chosen perpendicular to the $[M(OH)_2M]$ plane and along the $M-M$ vector, respectively; X corresponds approximately to the $O-O'$ direction. g_x and g_y were chosen bisecting the $N'-M-O'$, $N''-M-O$ and $N'-M-N''$, $O-M-O'$ angles, respectively, after projection into the $N'N''OO'$ plane; g_z is defined perpendicular to this plane. g_x , g_y , and g_z refer to the molecular g tensor of the CuN_3O_2 or VN_3O_3 polyhedron.

Table I. Crystal and Molecular Parameters of $[(L')Cu(OH)_2Cu(L')](ClO_4)_2$ (Ia) and $[(L)VO(OH)_2VO(L)]Br_2$ (II)^a

	Ia	II
space group	$P2_1/n^b$	$P2_1/c^b$
Lattice Parameters		
a , Å	20.41 (2)	7.236 (1)
b , Å	8.257 (4)	14.003 (2)
c , Å	8.671 (6)	10.405 (2)
β , deg	91.44 (6)	97.37 (2)
Interatomic Distances and Angles ^c		
$M-O$, Å	1.939 (9)	1.969 (5)
$M-O'$, Å	1.936 (4)	1.956 (5)
$M-N$, Å	2.238 (4)	2.303 (6)
$M-N'$, Å	2.083 (4)	2.159 (5)
$M-N''$, Å	2.060 (5)	2.151 (5)
$M-M$, Å	2.971 (1)	3.033 (1)
$\angle MOM$, deg	100.1 (2)	100.2 (2)

^aThe atom labeling refers to Figure 1. The data were taken from ref 10 and 11. ^bTwo differently oriented dimers in the unit cell. ^cThe additional $V-O''$ spacing is 1.603 (5) Å.

coupling model (second-order Jahn-Teller effect), which favors this geometry with respect to a compressed trigonal bipyramid.¹² The compound $[(L)VO(OH)_2VO(L)]_2Br_2$ (II) with the tridentate ligand 1,4,7-triazacyclononane (L) is to our knowledge the first example of a bis(μ -hydroxo)-bridged vanadium(IV) dimer. The bridge is again practically symmetrical, and the six-coordinated d^1 cations induce a distorted-octahedral environment with a very short $V-O''$ spacing and a long $V-N$ bond in the trans direction, which is typical for vanadium(IV) with an oxo ligand (Figure 1, Table I).

Since the structures in particular of the $[M(OH)_2M]$ core are very similar in both cases, there was the interesting opportunity to observe the dependence of the magnetic properties and zero-field splittings on the electronic structure for a d^9-d^9 in comparison to a d^1-d^1 dimer.

Experimental Section

Powder samples and single crystals of the complexes Ia, Ib, and II were kindly supplied by Prof. K. Wieghardt. Large single crystals suitable for electron spin resonance measurements could be easily grown from aqueous solutions.

The EPR spectra were recorded with a Varian E15 spectrometer supplied with a magnet operating over the range 500–25 000 G at about 9 and 35 GHz and in the temperature range 4.2–300 K. The Oxford Instruments and Varian low-temperature accessories were used at X and

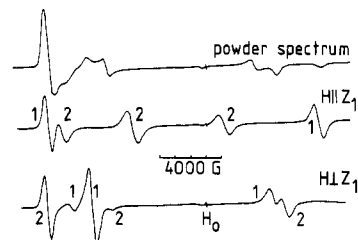


Figure 2. Powder and single-crystal spectra of $[(L')Cu(OH)_2Cu(L')](ClO_4)_2$ (Ia) at 80 K and 35.0 GHz ($H_0 = 12480$ G). The single-crystal spectra (rotation around " a ") show resonances due to the two differently oriented dimeric entities 1 and 2 in the unit cell.

Q frequencies, respectively. The electronic reflectance spectra at 298 K were measured with a Zeiss DMR-21 instrument for powder samples using Sr_2ZnTeO_6 and MgO as standards in the 4000–12 000 cm^{-1} and 8000–30 000 cm^{-1} ranges, respectively.

Results

Electronic Spectra. The blue copper dimer Ia shows two broad bands of nearly equal intensity at about 10 700 and 16 400 cm^{-1} , which may be tentatively assigned to the $A'(d_{x^2-y^2}) \rightarrow A'(d_{z^2})$ and $\rightarrow A'(d_{xy})$, $A''(d_{xz})$, $A''(d_{yz})$ transitions of the molecular CuN_3O_2 entities, respectively, in the apparent C_s point group. The latter band should not be split to a larger extent, because at least the triaza ligand is a pure σ donor. The corresponding transitions for the green dimer Ib are observed at somewhat lower energies. The two broad and also nearly equally intense bands appear at about 9000 and 15 700 cm^{-1} . Obviously the $d_{x^2-y^2}-d_{z^2}$ energy separation is lowered by 15%.

The ligand field spectrum of the binuclear vanadium complex II exhibits also two transitions, namely, at 14 200 and 19 400 cm^{-1} , the former with much higher intensity. An assignment to the transitions $A'(d_{xy}) \rightarrow A''(d_{xy})$, $A''(d_{yz})$ and $\rightarrow A'(d_{x^2-y^2})$, again in C_s symmetry, seems reasonable, while the transition to $A'(d_{z^2})$ is expected at considerably higher energies in the charge-transfer region.

EPR Spectra. Blue Cu(II) Dimer (Ia). The powder spectra taken at X- and Q-band frequencies showed characteristic spin-triplet state patterns (Figure 2). The spectra became less intensive when the temperature was lowered. Below 20 K the triplet spectrum disappeared completely. This behavior is in agreement with the results of magnetic investigations, which find an anti-parallel spin orientation of the two Cu^{2+} ions and hence also a $S = 0$ ground state.¹⁰ Below 20 K a weak spectrum of monomeric impurities can be observed, however, with $g_{\perp} \approx 2.06$, $g_{\parallel} = 2.25$, $A_{\perp} \approx 10 \times 10^{-4} cm^{-1}$, and $A_{\parallel} = 173 \times 10^{-4} cm^{-1}$. Since the dimerization affects only weakly the ligand field energies, we assumed the above values to be correct also for the dimer. This assumption is confirmed by the simulations. The covalency parameter, calculated from the orbital contributions to the g values on the basis of the ligand field energies, is $k \approx 0.77$. This value is reasonable for a mixed N,O-coordination.

The resonance lines in the single crystal experiments were rather broad at room temperature. The spectra measured at 80 K were of much better quality. A single crystal of the size $2 \times 1 \times 0.3 mm^3$ was used, which was rotated around the crystallographic axes a , b , c^* . The hyperfine structure could be not observed even at very low temperatures, similarly as reported for other hydroxo-bridged copper dimers.⁸ During the rotation around the a axis very well resolved spectra appeared (Figure 2). The resonances could be unambiguously assigned to the two differently oriented dimeric entities in the unit cell. Because of the morphology of the crystals the a axis could be oriented very accurately in the resonance cavity. If the crystals were rotated around b or c^* , the spectra due to the two dimers overlapped completely (for b) or approximately (for c^*) (see below). The angular dependencies of the spectra in the latter cases were extremely sensitive to small deviations of the rotation axis from the b or c^* directions. The distances between the signals were comparable to the line width in these orientations, and the interpretation of the spectra became difficult. We decided to extract the zero-field-splitting parameters

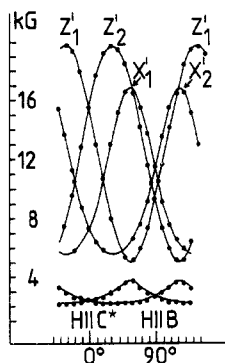


Figure 3. Angular dependencies of the resonance fields for $[(L')\text{Cu}(\text{OH})_2\text{Cu}(L')](\text{ClO}_4)_2$ (Ia) for the rotation of the crystal around the crystallographic a axis ($T = 80$ K, $\nu = 35.0$ GHz). At the orientations marked by "Z" the magnetic field deviates 5° from the Z axis of $\hat{\mathbf{D}}$ (Figure 1); at orientations marked by "X" the magnetic field deviates from the X and Y directions of $\hat{\mathbf{D}}$ by 23.2 and 66.8° , respectively. Experimental resonance fields (\bullet) and calculated angular dependencies (continuous lines) are given.

exclusively from the spectra measured in the bc^* plane (Figure 3)—and to use the angular dependencies for rotations around b or c^* only as an aid to confirm the results.

The EPR spectra of a spin-triplet state are described by the spin Hamiltonian¹³

$$\hat{H} = \beta \hat{H} \hat{g} \hat{S} + \hat{S} \hat{\mathbf{D}} \hat{S} \quad (1)$$

where $\hat{S} = \hat{S}_1 + \hat{S}_2$ is the total spin of the system and $\hat{\mathbf{D}}$ the zero-field splitting tensor. In a coordinate system where $\hat{\mathbf{D}}$ is diagonal, one can write

$$\hat{H} = \beta \hat{H} \hat{g} \hat{S} + D[\hat{S}_z^2 - \frac{1}{3}S(S+1)] + E(\hat{S}_x^2 - \hat{S}_y^2) \quad (2)$$

where

$$D = (2D_{zz} - D_{xx} - D_{yy})/2 \quad E = (D_{xx} - D_{yy})/2 \quad (3)$$

Thus, we fixed the coordinate system where we believed $\hat{\mathbf{D}}$ to be diagonal (Figure 1) and simulated the angular dependencies of the spectra in order to find the D and E parameters. We used the method of Baranowski et al.¹⁴ to calculate analytically the resonance fields at random orientation, without a need to diagonalize the matrix of (2). We adapted the equations given there for noncoaxial $\hat{\mathbf{D}}$ and $\hat{\mathbf{g}}$ tensors.¹⁴ The $\hat{\mathbf{g}}$ tensor was transformed to the coordinate system where $\hat{\mathbf{D}}$ is diagonal, which results in a nondiagonal matrix. Then the terms containing the g components were replaced:

$$\begin{aligned} l g_{xx} &\rightarrow l g_{11} + m g_{21} + n g_{31} \\ m g_{yy} &\rightarrow l g_{12} + m g_{22} + n g_{32} \\ n g_{zz} &\rightarrow l g_{13} + m g_{23} + n g_{33} \end{aligned} \quad (4)$$

l , m , and n are the direction cosines of the magnetic field vs. $\hat{\mathbf{D}}$. g_{xx} etc. are the components of the diagonal $\hat{\mathbf{g}}$ tensor, and g_{ij} are the components of the $\hat{\mathbf{g}}$ matrix when transformed to the $\hat{\mathbf{D}}$ coordinate system. The $\hat{\mathbf{g}}$ tensor was tentatively oriented as in Figure 1. It follows from experience that a choice of the g axes on the basis of the molecular (pseudo) symmetry usually gives very reasonable results. The coordinate system for the $\hat{\mathbf{D}}$ tensor was defined such that Y is the axis joining the copper ions and Z the axis perpendicular to the $[\text{Cu}(\text{OH})_2\text{Cu}]$ plane (Figure 1). Because the planes $[\text{Cu}(\text{OH})_2\text{Cu}]$ and $[\text{N}'\text{N}''\text{O}'\text{O}']$ are not parallel, the $\hat{\mathbf{D}}$ and $\hat{\mathbf{g}}$ tensors do not coincide. Using these coordinate systems, we find that the obtained D and E values are in very good agreement with the angular dependencies of either dimer in the unit cell. From the structural data a phase difference between

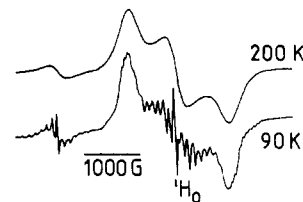


Figure 4. EPR powder spectra of $[(L)\text{VO}(\text{OH})_2\text{VO}(L)]\text{Br}_2$ (II) at 8.85 GHz ($H_0 = 3160$ G).

the two dimeric entities in the unit cell of 108° (72°) is deduced. We always observed 114° (66°), however (Figure 3). We may conclude that the true coordinate system for $\hat{\mathbf{D}}$ is only slightly different from the chosen one in Figure 1. Since the measured angular dependencies for both dimers are—besides the phase shift—completely identical we can improve the directional properties of the $\hat{\mathbf{D}}$ tensor by rotating the coordinate systems of the two dimers around the crystallographic a direction by 3° in the opposite sense. In contrast to the situation for $\hat{\mathbf{D}}$ small directional changes of the g axes affect only slightly the calculated angular dependencies. An excellent fit of the experimental angular dependencies of the EPR signals (Figure 3) was obtained with $|D| = 0.9250$ cm^{-1} and $|E| = 0.0514$ cm^{-1} . Though the absolute signs of D and E could not be determined, they were different for D and E . Difficulties were encountered, when the crystal was rotated in the ac^* or ab planes. A misorientation of only 2° in the position of the rotation axis, which is about the experimental uncertainty of the crystal orientation, caused a large shift of the resonances. The derived parameters are also in accord with the resonance fields for the powder spectra on the basis of the Wasserman equations.¹⁵ We did not try to simulate the powder patterns, however.

Green Cu(II) Dimer (Ib). The green isomer yielded an EPR powder spectrum with rather broad bands. The quality of the spectrum did not improve with decreasing temperature, but in contrast to the blue dimer the spectrum did not lose intensity on going to 4.2 K. This confirms the parallel spin orientation of the two Cu^{2+} ions in the dimeric entity and hence a $S = 1$ ground state, which was derived from magnetic susceptibility measurements.¹⁰ The single crystals either were too small or were of too bad quality in order to obtain well-defined EPR spectra. A rough estimation of the zero-field-splitting parameters from the powder spectrum yields 0.81 – 0.84 cm^{-1} for D , which is somewhat smaller than the corresponding value for the blue dimer. E is of about the same magnitude for the two isomers Ia and Ib.

V(IV) Dimer (II). The powder spectrum shows a rather atypical pattern with an intense central signal and a relatively strong half-field absorption (Figure 4). Also the zero-field splitting for the vanadium dimer seems to be much smaller than for the copper dimers. At temperatures lower than 200 K, a very nicely resolved hyperfine structure appeared. The hyperfine constant measured on the half-field transition is 84 G, which is approximately half of the A_z value for the monomer. At very low temperatures the dimer spectrum vanishes and a weak spectrum of monomeric impurities appears. An identical spectrum was found for the frozen DMF solution of the dimer. The parameters $g_{\parallel} = 1.945$, $g_{\perp} \approx 1.99$, $A_{\parallel} = 162 \times 10^{-4}$ cm^{-1} , and $A_{\perp} \approx 60 \times 10^{-4}$ cm^{-1} could be derived. Because g_{\perp} and A_{\perp} could not be extracted from the spectrum with high precision, we have estimated them by comparing the anisotropic frozen-solution and the isotropic liquid-solution spectra. The hyperfine splitting of the outer signals in the powder spectrum is smaller than the splitting of the central signal. This suggests that the latter is the "parallel" signal and the outer signals correspond to the "perpendicular" parameters. This sequence in the triplet spectrum is only possible, if D is small compared to E . The temperature dependence of the spectra is in this case also in accord with the magnetic result¹¹ of a $S = 0$ ground state. The well-resolved hyperfine structure

(13) Abragam, A.; Bleaney, B. *Electron Paramagnetic Resonance of Transition Ions*; Clarendon Press: Oxford, England, 1970.

(14) Baranowski, J.; Cukierda, T.; Jezowska-Trzebiatowska, B.; Kozłowski, H. *Chem. Phys. Lett.* **1976**, *39*, 606.

(15) Wasserman, E.; Snyder, L. C.; Yager, W. A. *J. Chem. Phys.* **1964**, *41*, 1763.

Table II. Direction Cosines of the Main Axes of the Zero-Field-Splitting and g Tensors with Respect to the Crystallographic a , b , c^* Axes for the Blue Cu(II) Dimer (Ia)

	\hat{D}^a			\hat{D}_{dip}			\hat{g}		
x	0.3916 (0.3947)	0.7278 (0.7551)	0.5630 (0.5235)	0.3896	0.7196	0.5247	0.3928	0.7185	0.5739
y	0.9172 (0.9159)	-0.3576 (-0.3689)	-0.1757 (-0.1585)	-0.9179	0.3588	0.1738	0.9196	-0.3100	-0.2413
z	0.0734 (0.0734)	0.5852 (0.5420)	-0.8076 (-0.8372)	0.0764	0.5955	-0.8001	0	0.6225	-0.7826

^aThe data in parentheses refer to the coordinate system for \hat{D} after rotation by 3° around the a axis (see text).

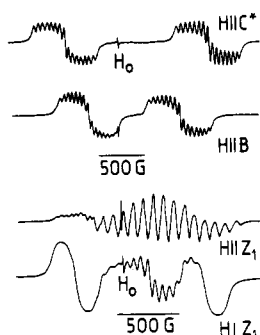


Figure 5. Single-crystal EPR spectra for $[(L)VO(OH)_2VO(L)]Br_2$ (II) at 34.90 GHz and 150 K ($H_0 = 12450$ G). Note the different scales for the upper and lower plots.

in the dimer spectrum below 200 K is obviously the result of only a small population of the excited $S = 1$ state and hence a considerable diamagnetic dilution by dimers with $S = 0$.

The single-crystal spectra measured at $H \parallel b$, $H \parallel c^*$ and at the approximate orientations $H \parallel Z_1$, $H \perp Z_1$ found by rotation around the c^* axis are displayed in Figure 5. The subscripts 1 and 2 again refer to the two differently oriented dimers in the unit cell. The directions $H \parallel b$ and $H \parallel c^*$ could be found very precisely ($\pm 1^\circ$) by rotating the crystal around the a axis, because the signals due to the two dimeric units exactly overlap at these orientations. The angular dependencies of the resonance fields could not be derived as accurately as for the blue copper dimer, because the hyperfine splitting and the zero-field-splitting parameter D are of comparable magnitude. The spectra were analyzed analogously to those of the blue copper dimer, and the following spin Hamiltonian parameters could be extracted:

$$g_x^c = 1.988 \quad g_y^c = 1.975 \quad g_z^c = 1.946$$

$$A_x^c = 23 \times 10^{-4} \text{ cm}^{-1} \quad A_y^c = 32 \times 10^{-4}$$

$$A_z^c = 76 \times 10^{-4} \text{ cm}^{-1}$$

$$|D| = 0.0037 \quad |E| = 0.0472 \text{ cm}^{-1}$$

The D and E parameters have the same sign and refer to a coordinate system analogous to the one for the blue copper dimer (Figure 1). The directions of the \hat{g} components are also defined in the same way.

Discussion

The zero-field-splitting tensor for exchange-coupled $S = 1/2$ ions contains contributions due to magnetic dipole-dipole and exchange interactions:

$$\hat{D} = \hat{D}^{\text{dip}} + \hat{D}^{\text{ex}} \quad (5)$$

The dipolar part of the zero-field-splitting tensor can be calculated by using the formula of Smith and Pilbrow,¹⁶ which has a very simple form for a centrosymmetrical dimer:

$$D_{\alpha\gamma}^{\text{dip}} = 1/2 g_\alpha g_\gamma (\delta_{\alpha\gamma} - 3\sigma_\alpha \sigma_\gamma) \beta^2 / r^3 \quad (6)$$

(Note that a factor $1/2$ has to be added to the equation¹⁶ dealing with the $S_1 \hat{D} S_2$ Hamiltonian, if the Hamiltonian is applied in the

form $\hat{S} \hat{D} \hat{S}$.) The σ_i variables are the direction cosines between the vector joining the two metal ions and the direction of g_i ($i = x, y, z$); δ_{ij} is Kronecker's δ function.

Blue Cu(II) Dimer (Ia). The calculated tensor \hat{D}^{dip} is expressed in the system of the main axes of \hat{g} and is not diagonal

$$\hat{D}^{\text{dip}} = \begin{Bmatrix} 2.130 & -0.016 & 0.001 \\ -0.016 & -4.218 & 0.561 \\ 0.001 & 0.561 & 2.481 \end{Bmatrix} \cdot \beta^2 / r^3$$

yielding after diagonalization

$$D_{xx}^{\text{dip}} = 0.035 \text{ cm}^{-1} \quad D_{yy}^{\text{dip}} = -0.071 \text{ cm}^{-1}$$

$$D_{zz}^{\text{dip}} = 0.042 \text{ cm}^{-1}$$

or when eq 3 is applied $D^{\text{dip}} = 0.060 \text{ cm}^{-1}$, $E^{\text{dip}} = 0.053 \text{ cm}^{-1}$. The largest component of \hat{D} refers to the vector that connects the two Cu^{2+} ions. Since the main axes of the dipole-dipole interaction tensor and the axes of the zero-field-splitting tensor (Figure 1) are nearly parallel (Table II), we can easily deduce the exchange contributions from the experimental D and E values ($D = -(+)0.9250 \text{ cm}^{-1}$, $E = +(-)0.0514$). There are two alternatives concerning the sign. We have chosen the first, because it yields the expected negative sign for D_{zz}^{Ex} .¹⁻⁴

$$D_{xx}^{\text{Ex}} = 0.325 \text{ cm}^{-1} \quad D_{yy}^{\text{Ex}} = 0.328 \text{ cm}^{-1}$$

$$D_{zz}^{\text{Ex}} = -0.659 \text{ cm}^{-1}$$

or $D^{\text{Ex}} = -0.985 \text{ cm}^{-1}$, $E^{\text{Ex}} = -0.002 \text{ cm}^{-1}$.

The D_{ii}^{Ex} values ($i = x, y, z$) are the components of the traceless tensor \hat{D}^{Ex} ($\sum D_{ii}^{\text{Ex}} = 0$) and have been deduced by applying eq 3. The vanishing E^{Ex} value demonstrates that the exchange interactions have axial symmetry. This is not unexpected, because the symmetry of the $[\text{Cu}(\text{OH})_2\text{Cu}]$ bridge is high.

The exchange-induced part of the zero-field splitting is due to the interaction of the two Cu^{2+} ground-state wave functions, which are mainly of $d_{x^2-y^2}$ character. Contributions of the excited states d_{xy} , d_{xz} , and d_{yz} are admixed via LS coupling, however. The components of the corresponding \hat{D}^{ex} tensor can be expressed in terms of the involved exchanged integrals $J_{x^2-y^2,j}$ ($j = xy, xz, yz$):

$$D_{xx}^{\text{ex}} = 1/8 (\Delta g_x)^2 J_{x^2-y^2,yz} \quad D_{yy}^{\text{ex}} = 1/8 (\Delta g_y)^2 J_{x^2-y^2,xz} \quad (7)$$

$$D_{zz}^{\text{ex}} = 1/32 (\Delta g_z)^2 J_{x^2-y^2,xy}$$

It must be borne in mind that one obtains from experiment always a traceless tensor (\hat{D}^{Ex}), whereas eq 7 refers to a nontraceless tensor (\hat{D}^{ex}). The relations between the respective components are

$$D_{xx}^{\text{Ex}} = 2/3 D_{xx}^{\text{ex}} - 1/3 D_{yy}^{\text{ex}} - 1/3 D_{zz}^{\text{ex}}$$

$$D_{yy}^{\text{Ex}} = -1/3 D_{xx}^{\text{ex}} + 2/3 D_{yy}^{\text{ex}} - 1/3 D_{zz}^{\text{ex}}$$

$$D_{zz}^{\text{Ex}} = -1/3 D_{xx}^{\text{ex}} - 1/3 D_{yy}^{\text{ex}} + 2/3 D_{zz}^{\text{ex}} \quad (8)$$

Because D^{ex} cannot be expressed by D^{Ex} , some reasonable assumptions have to be made, in order to obtain the components of D^{ex} and hence the exchange integrals $J_{x^2-y^2,j}$. Presumably $J_{x^2-y^2,xz}$ and $J_{x^2-y^2,yz}$ are small with respect to $J_{x^2-y^2,xy}$,^{1-4,17-19} i.e. D_{xx}^{ex} and

(17) Kahn, O.; Galy, J.; Journaux, Y.; Jaud, J.; Morgenstern-Badarau, I. *J. Am. Chem. Soc.* **1982**, *104*, 2165.

(18) Boillot, M. L.; Journaux, Y.; Bencini, A.; Gatteschi, D.; Kahn, O. *Inorg. Chem.* **1985**, *24*, 263.

(19) Julve, M.; Verdager, M.; Charlot, M. F.; Kahn, O.; Claude, R. *Inorg. Chim. Acta* **1984**, *82*, 5.

Table III. Direction Cosines of the Main Axes of the Zero-Field-Splitting and g Tensors with Respect to the Crystallographic a , b , c^* Axes for the V(IV) Dimer (II)

	\hat{D}			\hat{D}_{dip}			\hat{g}		
x	0.5597	-0.8273	0.0477	0.5597	-0.8273	0.0477	0.5585	-0.8281	0.0479
y	0.0683	0.1034	0.9923	0.0690	0.1038	0.9919	0.2500	0.2231	0.9422
z	-0.8259	-0.5522	0.1144	-0.8264	-0.5507	0.1151	-0.7909	-0.5143	0.3316

D_{yy}^{ex} must also be small. On the other hand, we derived from experiment that they are nearly equal, though there is no way to find their absolute magnitudes. For vanishing values of D_{xx}^{ex} and D_{yy}^{ex} one obtains from eq 7 and 8

$$D_{zz}^{\text{Ex}} = 1/48(\Delta g_z)^2 J_{x^2-y^2,xy}$$

An exchange integral $J_{x^2-y^2,xy} \simeq -510 \text{ cm}^{-1}$ is calculated with the above assumptions.

V(IV) Dimer (II). A similar treatment as for the Cu(II) dimer leads to

$$\hat{D}^{\text{dip}} = \begin{Bmatrix} 1.976 & 0 & 0 \\ 0 & -7.226 & 2.494 \\ 0 & 2.494 & 3.228 \end{Bmatrix} \beta^2/r^3$$

and after diagonalization

$$D_{xx}^{\text{dip}} = 0.031 \text{ cm}^{-1} \quad D_{yy}^{\text{dip}} = -0.060 \text{ cm}^{-1} \\ D_{zz}^{\text{dip}} = 0.029 \text{ cm}^{-1}$$

or $D^{\text{dip}} = 0.043 \text{ cm}^{-1}$ and $E^{\text{dip}} = 0.046 \text{ cm}^{-1}$.

Again the main axes of \hat{D}^{dip} have nearly the same orientation as \hat{D} (Figure 1). The largest component is along the V-V vector (Table III). From the experimental values— D and E were chosen with a positive sign to give a negative D_{zz}^{Ex} contribution—we calculate

$$D_{xx}^{\text{Ex}} = 0.015 \text{ cm}^{-1} \quad D_{yy}^{\text{Ex}} = 0.012 \text{ cm}^{-1} \\ D_{zz}^{\text{Ex}} = -0.027 \text{ cm}^{-1}$$

or $D^{\text{Ex}} = -0.041 \text{ cm}^{-1}$ and $E^{\text{Ex}} = 0.002 \text{ cm}^{-1}$. Again the exchange interactions have axial symmetry.

From the equations given in ref 5–8 we have deduced the following relations between the D^{ex} tensor components and the exchange integrals $J_{xy,j}$ ($j = x^2 - y^2, xz, yz$), which refer to the d^1 -configured V(IV) ion in an axially compressed octahedron (Table I):

$$D_{xx}^{\text{ex}} = 1/8(\Delta g_x)^2 J_{xy,xz} \quad D_{yy}^{\text{ex}} = 1/8(\Delta g_y)^2 J_{xy,yz} \\ D_{zz}^{\text{ex}} = 1/32(\Delta g_z)^2 J_{xy,x^2-y^2} \quad (9)$$

With the assumption of vanishing $J_{xy,xz}$ and $J_{xy,yz}$ exchange integrals, in analogy to the case of the blue Cu(II) dimer, one estimates

$$J_{xy,x^2-y^2} \simeq -410 \text{ cm}^{-1}$$

Possibly the error of this value is considerably larger than in the case of the copper dimer. On the one hand, the exchange contribution to the zero-field splitting is of the same order of magnitude as the dipolar one, while in the copper dimer it is the dominating component. On the other hand, Δg_z is quite small in this case and already a small uncertainty in this value may introduce a large error.

It is very instructive to compare the exchange integrals derived from magnetic susceptibility data^{10,11} with those from our EPR data:

$$\text{Cu(II) dimer Ia: } J_{x^2-y^2,x^2-y^2} \simeq 90 \text{ cm}^{-1}, J_{x^2-y^2,xy} \simeq -510 \text{ cm}^{-1}$$

$$\text{V(IV) dimer II: } J_{xy,xy} \simeq 354 \text{ cm}^{-1}, J_{xy,x^2-y^2} \simeq -410 \text{ cm}^{-1}$$

The integrals $J_{x^2-y^2,x^2-y^2}$ and $J_{xy,xy}$ correspond to the metal-metal interaction, which is described by the Hamiltonian $\hat{H} = J\hat{S}_1\hat{S}_2$. They are equal to the triplet-singlet separation with a plus sign for antiferromagnetic interactions. These two integrals are drastically different, while the J integrals derived from the zero-field splittings are of comparable magnitude. The difference between $J_{x^2-y^2,x^2-y^2}$ and $J_{xy,xy}$ can be easily rationalized, because only the latter implies a direct overlap of orbitals. $J_{x^2-y^2,xy}$ and J_{xy,x^2-y^2} , on the other hand, are indeed expected to be similar, if one disregards the different charges of the metal ions and the slightly different metal-metal spacings.

Conclusions

The contributions of the dipole-dipole and exchange interactions to the zero-field-splitting parameters in the dimeric copper (Ia) and vanadium complexes (II) have been calculated from the experimental data. The E parameter of the spin Hamiltonian has been found to be of nearly exclusive dipole-dipole nature. It is very similar for the copper and vanadium dimers, whereas the D parameter contains contributions due to both dipolar and exchange interactions. The exchange component is dominant for the copper compound, yielding a large value of D , while it is of the same order of magnitude as the dipolar component for the vanadium dimer. The dipolar and exchange parts of D nearly cancel in the latter case, and a very small D value results. The exchange integrals $J_{x^2-y^2,xy}$ and J_{xy,x^2-y^2} , which were estimated from the zero-field-splitting parameters and the g anisotropies, are found to be of similar magnitude for the d^9 - d^9 (Ia) and d^1 - d^1 dimers (II), respectively, in accord with symmetry-equivalent exchange pathways. The isotropic exchange integral $J_{x^2-y^2,x^2-y^2}$ (for Ia) is much smaller than $J_{xy,xy}$ (for II), however (both values have been deduced from susceptibility measurements^{10,11}), because only the latter implies a direct overlap between metal d orbitals.

Safety Notes. Perchlorate salts of metal complexes with organic ligands are potentially explosive. In general, when noncoordinating agents are required, every attempt should be made to substitute anions such as the fluoro sulfonates for the perchlorates. If a perchlorate must be used, only small amounts of material should be prepared and this should be handled with great caution.

Acknowledgment. It is a pleasure for us to thank Prof. K. Wieghardt and Dr. P. Chaudhuri (University of Bochum) for having provided the dimer compounds and for discussions. Financial support by the "Deutsche Forschungsgemeinschaft" (SFB 127: Kristallstruktur und chemische Bindung) is gratefully acknowledged.

Registry No. Ia, 93806-56-5; II, 89178-84-7.